Delft University of Technology

Comb mode filtering silver mirror cavity for spectroscopic distance measurement

Šmíd, R.; Hänsel, A.; Pravdová, L.; Sobota, J.; Cíp, O.; Bhattacharya, N.

Important note
To cite this publication, please use the final published version (if applicable).
Please check the document version above.

Comb mode filtering silver mirror cavity for spectroscopic distance measurement

R. Šmíd, A. Hänsel, L. Pravdová, J. Sobota, O. Číp, and N. Bhattacharya

Comb mode filtering silver mirror cavity for spectroscopic distance measurement

R. Šmíd,[1,a)] A. Hänsel,[2] L. Pravdová,[1] J. Sobota,[3] O. Číp,[1] and N. Bhattacharya[2]

[1]*Department of Coherence Optics, Institute of Scientific Instruments of the CAS, v.v.i.,*
61264 Brno, Czech Republic
[2]*Department of Imaging Physics, Faculty of Applied Sciences, Delft University of Technology,*
2628 CJ Delft, Netherlands
[3]*Department of New Technologies, Institute of Scientific Instruments of the CAS, v.v.i.,*
61264 Brno, Czech Republic

In this work we present a design of an external optical cavity based on Fabry-Perot etalons applied to a 100 MHz Er-doped fiber optical frequency comb working at 1560 nm to increase its repetition frequency. A Fabry-Perot cavity is constructed based on a transportable cage system with two silver mirrors in plano-concave geometry including the mode-matching lenses, fiber coupled collimation package and detection unit. The system enables full 3D angle mirror tilting and x-y off axis movement as well as distance between the mirrors. We demonstrate the increase of repetition frequency by direct measurement of the beat frequency and spectrally by using the virtually imaged phased array images. *Published by AIP Publishing.* [http://dx.doi.org/10.1063/1.4962681]

I. INTRODUCTION

The development of the optical frequency comb as a referenced light source has increased the precision in many metrology applications. The accurate and stable frequency reference provides advantages in many fundamental experiments[1,2] while parallelly being used in applications ranging from improving the accuracy of astronomical spectrographs[3,4] as well as the detection of molecular markers in human breath.[5] Another advantage that the optical frequency comb laser source offers is the extraordinary phase stability between the pulses of the laser. This has been exploited in length metrology by implementing a new generation of techniques and achieving very high accuracies. The techniques range from using the ultra-stable inter-pulse distance of the source,[6,7] frequency modulation based measurements,[8] multi-heterodyne measurements,[9] time of flight measurements,[10] and spectral interferometry.[11,12] Spectral interferometry using the large spectral bandwidth of the frequency comb, where the illumination can be considered to be made up of thousands of stable lasers makes possible real time monitoring of optical lengths. The Virtually Imaged Phased Array (VIPA) was the first spectrometer to experimentally demonstrate resolved frequency comb spectra[13,14] but soon other techniques mainly based on Fourier transform spectroscopy, like the dual comb spectroscopy[15] or regular FTIR spectroscopy[16] took over. The VIPA spectrometer has the advantage of a compact setup, on the detector side with no moving parts and simple electronics.[13,17,18] The VIPA spectrometers were initially developed to work with the Ti:Sapphire oscillator-based (Ti:Sapph) frequency combs which had repetition rates larger than 1 GHz. These laser sources, which were also the first to be converted to frequency combs were excellent in coherence properties but they were large and more difficult to maintain for long term stability. The resolution of the VIPA was sufficient for separating the individual spectral modes of the frequency comb, supporting a massively parallel homodyne interferometry method for the Ti:Sapph based combs.[18] A new generation of frequency combs based on Erbium or Ytterbium doped fibers[19,20] were soon developed which were compact, stable, and easily transportable. The repetition rates of these lasers were sub-GHz, mostly being in hundreds of MHz and the VIPA spectrometer was no longer so effective in resolving the laser modes of these new frequency combs. This is a serious drawback since these compact combs can be easily transported for field measurements, sent on satellites and used in hazardous environments. The combination with a compact non-moving spectrometer would be very useful for field and industrial applications. In this paper, we report the development of an external filter cavity[19,21,22] which increases the mode spacing of the fiber based combs such that a VIPA spectrometer can resolve them for applications in long distance measurement. The cavity has been used to increase the mode spacing of an Er-doped fiber based frequency comb with a repetition rate of 100 MHz to 1 GHz, well beyond the resolution limit, 680 MHz, of the VIPA spectrometer. Using this setup, the advantages of massively parallel homodyne interferometry can be exploited for applications in outdoor distance measurements.

II. EXPERIMENTAL SETUP

The principle of the method developed is based on the simple idea of the multiplication of initial repetition frequency of a femtosecond mode-locked laser or an optical comb. The frequency of each comb line can be described by the following basic relation:

$$f_i = f_0 + i \cdot f_{\rm rep}, \tag{1}$$

a)Electronic mail: smradeksm@gmail.com.

where f_0 is the offset frequency representing the phase delays inside the initial comb cavity and f_{rep} is the repetition frequency of the laser. The multiplication of the repetition frequency f_{rep} can be done by an external cavity with two mirrors in Fabry-Perot configuration only under some restrictions. The first restriction concerns the free spectral range (FSR) of the Fabry-Perot cavity $\Delta\nu_{FSR}$ that should be the multiple of the initial comb repetition frequency,

$$\Delta\nu_{FSR} = m \cdot f_{rep}. \tag{2}$$

Here, for $\Delta\nu_{FSR}$[23] in plano-concave configuration and mirror distance L_{cav} we have

$$\Delta\nu_{FSR} = \frac{c}{2 \cdot n_{air}L_{cav}}\left(1 + \frac{\delta}{2\pi} \cdot \frac{c}{n_{air}L_{cav}}\right)^{-1}. \tag{3}$$

In the above relation, n_{air} is the refractive index of air between mirrors and δ is the coefficient representing the chromatic dispersion on the cavity mirrors. The second restriction is on the phase delay during the round trip in the cavity. In an optically dispersive cavity, chromatic dispersion will cause different wavelengths to acquire different phase delays in the cavity. The chromatic dispersion delay has two components, the delay on the mirrors τ_m (the phase delay δ) and the delay in the medium, in this case, air between mirrors (τ_{air}). We aimed to control these two restrictions in this design. The schematic of the complete experimental setup is shown in Fig. 1. The source laser is a Er-doped femtosecond laser with repetition frequency of 100 MHz working at the wavelength range from 1500 to 1600 nm and consists of free space infra-red optical high power output of ~100 mW. For our experiments, the free space output was collimated via a 200 mm focal length lens and directed using a pair of silver mirrors to the in-coupler of a single-mode fiber. The output from the collimator at the fiber exit was further focused by a mode-matching cavity lens onto the Fabry-Perot cavity (FPC). The FPC design consists of silver mirrors on stainless steel rods of a commercially

available cage system and precision mirror mounts for coarse FSR alignment. The piezoelectric transducer (PZT) has been used for fine adjustment of FSR to the femtosecond frequency comb repetition frequency and to compensate the temperature and environmental drifts of the cavity. The output of the femtosecond laser beam from the cavity was split by 50/50 on a non-polarized prism to a control part and an output analysis part. The control part includes a photodetector (PD) and servo-loop electronics to control the voltage of the PZT to be able to lock the FPC length to the frequency comb mode resonance. The output analysis part measures the efficiency of the initial frequency comb repetition frequency multiplication process. The analysis of the FPC output signal consists of two independent optical systems separated by the steering silver mirror that switched between two optical paths. The first one analyzed the beat note frequency RF spectrum among the passing comb modes with the fast photodetector FPD and RF spectrum analyzer. The second one consisted of the optical setup where the beam is focused with the slit and cylindrical lens onto the input window of the Virtually Imaged Phased Array (VIPA) and the diffraction grating where the frequency comb modes were separated and expanded spatially on the infrared 2D matrix IR CCD camera. The intensity spectral pattern captured by IR CCD camera was saved, post-processed, and analyzed.

III. CAVITY DESIGN

The key part of the setup has been the design of the cavity, its mechanical components, and the voltage control of the mirror position by the PZT. The frequency comb laser has an initial repetition frequency of 100 MHz. Our goal was to increase the repetition frequency of the laser. The repetition frequency of 1 GHz has been chosen for the 10th multiple of the initial frequency. The resulting mode-spacing is large enough to be resolved by the VIPA and can still be determined
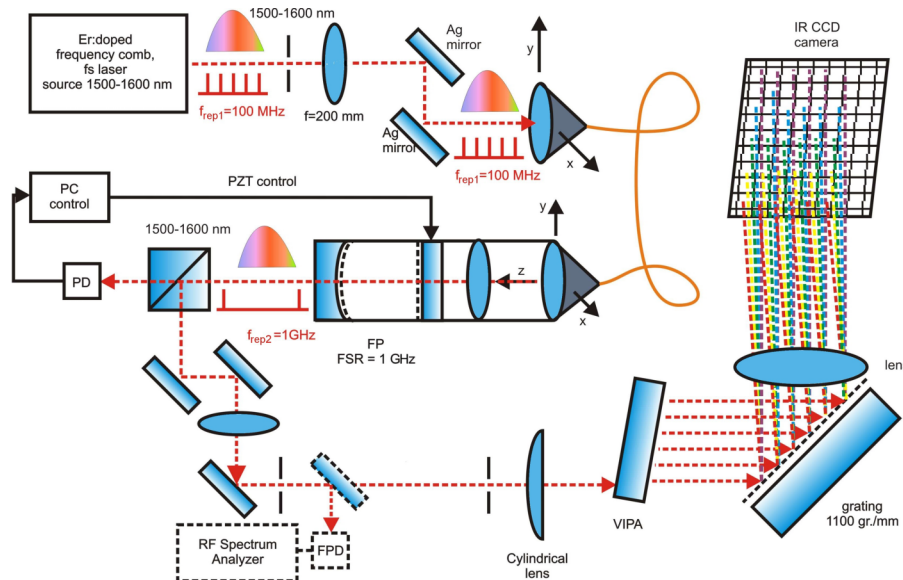

FIG. 1. Scheme of setup: FP—Fabry-Perot, PD—photodetector, PZT control—piezo-electric transducer, detection part: IR CCD—infra-red camera, VIPA—virtually image phased array etalon, FPD—fast photodetector.

by the fast photodiode. This choice left us with enough power for practical applications since the FPC of 1 GHz FSR would theoretically lead to a decrease to 1/10th of the initial optical power.

A. Mechanical setup

The construction of the repetition frequency multiplying FPC with FSR of 1 GHz was based on standard 30 mm and 60 mm cage holder stainless steel rod systems from Thorlabs Inc. and several mirror holders of 30 mm and 60 mm with 3D positioning systems enabling the rotation of the angle and the coarse position of the mirrors in the cavity. One mirror was set into an aluminum cylindrical holder with PZT for fine mirror position. The PZT material was Ferroperm Pz27 cylindrical tube with an outer diameter of 20.5 mm, inner diameter of 18.5 mm and the length of 14 mm. The electrical connection was supplied with electrodes on the tube walls which could provide ±280 V, to enable tube length displacement of up to more than a half-wavelength of the central wavelength of the frequency comb laser. At first, the cavity was aligned using a visible laser source: a tunable helium-neon laser working at 632.8 nm. This was an advantage when using the silver mirror cavity due to a wide wavelength range used in the visible and the infrared parts of the spectrum. The second step of alignment was done by using a very narrow tunable laser working at 1540 nm (ORION laser module) with <3 kHz linewidth. This laser was aligned and locked to the TEM_{00} mode of the Fabry-Perot cavity by the first derivative technique using the ramp length modulation of the piezo-ceramic transducers on the flat mirror holder.

The frequency comb laser light in the wavelength range of 1500-1600 nm is subsequently injected into the same setup. The laser light entering the cavity is delivered via an infrared collimator and the single-mode fiber. Because the cavity was already aligned for the 1540 nm single mode laser, it only needs to be precisely moved to the position where it matches the condition in Eq. (2). The exact length was roughly determined by a simple ruler but for more exact positioning, we added CXYZ1/M-XYZ Translation Mount and the lock was achieved with help of the PZT tube and the loop in the controller. Fig. 2 shows the design of the cavity.

The cavity was set up based on the input beam parameters. The cavity configuration was plano-concave. This was chosen in order to keep the input modes from degenerating inside the cavity. The input mirror M_1 was flat and the output mirror M_2 was set to 150 mm from the first one and had radius of

curvature of 800 mm. The laser modes were mode matched to the cavity[23] with a lens pair, with focal lengths of 200 mm and 150 mm, placed in front of the input mirror. The beam waist at the input mirror was 390 μm. Errors in beam focal lengths caused by the difference in refractivity of glass of mode-matching lenses made from BK7 glass for 1500 nm and 1600 nm was around $3 \cdot 10^{-3}$. The corresponding relative difference in the beam waist radius for both wavelengths was negligible $4 \cdot 10^{-6}$. The diameter of mirror apertures has been chosen to 12.3 mm which is larger than the exiting beam diameter based on Gaussian beam theory. The cavity has been constructed at the Institute of Scientific Instruments (ISI) from the standard Thorlabs parts with the aim of ease of transportability.

B. Influence of ambient environmental changes on the cavity

The cavity between the mirrors is filled with the ambient air and the cavity was covered with the polystyrene box to block surrounding air flow and sudden turbulence in the air flow. Using Bönsch and Potulski's updated Edlen's equation of refractive index of air,[24] we estimated the influence of the environmental parameters on the refractive index of air for the wavelength range 1500–1600 nm. The temperature variation in the room was between 19 °C and 22 °C leading to the temperature variation component being $1.1 \cdot 10^{-6} \, K^{-1}$, where the difference of refractive index of air for two extreme wavelengths is $-9 \cdot 10^{-8}$. A relatively large humidity variation from 10% to 90% gives only a refractive index variation of $2 \cdot 10^{-7}$. The weather data show that pressure variation over a week under relatively stable condition is less than 15 hPa, this corresponds to relative change of refractive index of air of $3 \cdot 10^{-7}$. Thus the cavity is most sensitive to temperature variations of the refractive index of air. The temperature in the laboratory can be easily controlled, usually under laboratory conditions it has not varied more than 1 °C, thus the relative variation of the cavity of 10^{-6} is quite realistic. The cavity length was 150 mm, thus the temperature variation of the air in the cavity corresponds to the 150 nm length variation of the cavity.

Stainless steel rods (stainless steel type 303) were used in the cavity construction. The length of the rods was 150 mm. With the thermal expansion coefficient of stainless steel of $\approx 1.73 \cdot 10^{-5} \, m^{-1}K^{-1}$ and temperature variations of 1 K, the cavity length can vary up to 2.6 μm. The typical thermal expansion coefficient of the piezo-ceramics vary
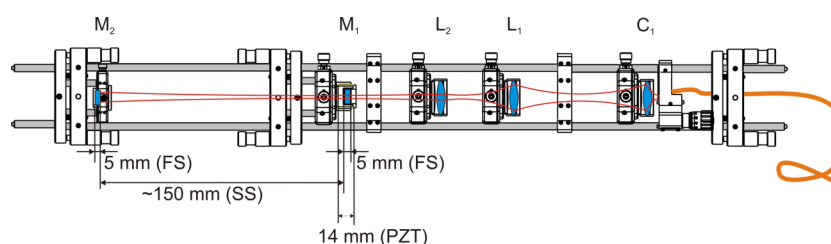

FIG. 2. Design of the cavity based on the on stock Thorlabs components: C_1—fiber collimator with lens, L_1, L_2—mode-matching lenses, M_1—flat cavity mirror, M_2—curved cavity mirror, FS—fused silica, PZT—PZT transducer ceramics, SS—stainless steel.

TABLE I. Temperature (T), humidity (h) and pressure (p) contributions to cavity displacement.

Nature	rel.eff.	tot. eff.	abs. length/nm
Air			
T	$1.1 \cdot 10^{-6} \, K^{-1}$	10^{-6}	150
h	...	$2 \cdot 10^{-7}$	30
p	$2 \cdot 10^{-8} \, hPa^{-1}$	$3 \cdot 10^{-7}$	45
Material/K			
Rods	$1.73 \cdot 10^{-5}$	$1.73 \cdot 10^{-5}$	+ 2595
PZT	$10^{-5} - 10^{-6}$	10^{-6}	−140
Al	$2.2 \cdot 10^{-5}$	10^{-6}	+132
m. subst.	$5.5 \cdot 10^{-7}$	$3.6 \cdot 10^{-8}$	−5.5

from $10^{-6} \, m^{-1} K^{-1}$ to $10^{-5} \, m^{-1} K^{-1}$ and the typical value for aluminum is $2.2 \cdot 10^{-5} \, m^{-1} K^{-1}$. The cavity was designed and constructed such that the temperature dependent length changes of the PZT holder (PZT) and PZT tube transducer as shown in Fig. 2, are in opposite direction and the total contribution subtract as seen in Table I. The PZT tube was 10 times shorter than the total cavity length thus the total contribution to the cavity length changes is of the order of the temperature variation of air and under the order of the variation of the stainless steel rods (rods). The thermal expansion coefficient of the pair of fused silica mirror substrates (m. subst.) of total thickness of 10 mm is $5.5 \cdot 10^{-7} \, m^{-1} K^{-1}$ and this yields to total length change of 5.5 nm with 1 K temperature variations. Thus the potential length change of the cavity should be compensated. In our setup, the PZT transducer lock worked as the cavity length compensator within the range of applied voltage up to ±280 V or 1.333 μm that is according to our previous calculation sufficient for up to 0.5 K temperature changes of air. Thus the cavity needs to be relocked in case of larger changes of temperature.

C. Cavity mirrors

Another aspect taken into consideration in the cavity design was the mirror quality and the intra-cavity loss and dispersion. The goal was to minimize the intra-cavity loss, loss on the mirror substrates, the dispersion and group velocity delay of the beam during round-trips in the cavity. To lock the cavity to the frequency comb the factors that effect the dispersion inside the cavity due to the refractive index of air with a value above $-9 \cdot 10^{-8}$. The model for refractive index of air—n_{air} = 1.000 273 25. The model for refractive index of air (dry air at 15 °C, 101 345 Pa and 450 pm CO_2 content) at 1560 nm based on the Sellmeier equation and Ciddor's data[25] results in:

- refractive index of air—n_{air} = 1.000 273 25.
- Chromatic dispersion—$dn_{air}/d\lambda$ = $-8.1320 \cdot 10^{-7} \mu m^{-1}$.
- Group velocity dispersion—GVD = 1.0734 $fs^2 m^{-1}$ thus the dispersion parameter $D_\lambda = -2\pi c / \lambda^2 \cdot$ GVD = 0.830 83 ps/(nm km).

From the last relation, it can be seen that the 100 nm wide spectrum from the laser in the 0.15 m long cavity leads to a dispersion of 12.5 fs for the light pulse in the cavity in one round trip. The total dispersion of the pulse depends also on the finesse of the cavity and thus the number of round-trips in the cavity. For a finesse value F of around 200, it can lead up to 2.5 ps of pulse dispersion. For considering the complete traversal of the femtosecond pulse through the cavity, we must take the single pass through each mirror substrate into account. The typical fused silica mirror has its GVD = $-300 \, fs^2 cm^{-1}$ at central wavelength of 1560 nm, this corresponds to 20 ps/(nm km). Hence if the spectrum is 100 nm wide and the total thickness of the mirror substrates is 1 cm, the estimated pulse delay will be 20 fs.

The material of the mirrors plays the crucial role in the design of the cavity. The typical dielectric mirrors for broadband application have about 100 fs^2 (low dispersion mirrors <30 fs^2), thus the delay for the 100 nm broad spectrum from 1500 nm to 1600 nm is below 1 fs and thus leads to a total delay of 200 fs for a typical pulse in the cavity. The comparison of different types of mirror materials and their contribution to the total pulse delay in the cavity is shown in Table II.

The dielectric mirrors usually consist of several dielectric layers of several μm thicknesses. These mirrors enable different penetration depths for various optical wavelengths.[26] In contrast, metal mirrors have very low dispersion and almost no group velocity dispersion[27] because they consist of a single layer. We chose silver mirrors because of good reflectivity compared to gold within wide optical band. The critical parameters in the metal cavity mirrors are their optical properties in visible and infrared optical spectra hence the wavelength dependent transmission through the metal layer. Based on Beer-Lambert's law, the penetration depth of the incident light perpendicular to the surface is indirectly proportional to the absorption coefficient α of the material. The intensity of the electric field I_0 decreases exponentially with α, i.e., $I = I_0 \cdot \exp(-\alpha)$. Another limiting factor is the lowest achievable homogeneous metal layer. According to models based on experimental data sets and the Brendel-Bormann model,[28,29] we can estimate that the real part of the refractive index of silver n_{Ag} and its imaginary part k_{Ag} corresponding to the absorption in the material varies from $\tilde{n}_{Ag} = n_{Ag} + i \cdot k_{Ag}$ = $0.39008 + i \cdot 9.7154$ to $\tilde{n}_{Ag} = 0.42980 + i \cdot 10.380$. Here the imaginary part k_{Ag} controls the optical field penetration into the metal and the real part is responsible for the phase delay of the electric field. The penetration depth $1/\alpha$ is dependent on the wavelength.

Based on Fresnel's equation, the calculation for the 40 nm thick silver coating on fused silica for a 1540 nm

TABLE II. Pulse dispersion estimation, m. subst.—mirror substrates, dm—dielectric mirrors, NGVD m.—negative group velocity dispersion mirrors, metal m.—metal mirrors, mp—multi-pass, GVD—group velocity dispersion, D_λ—dispersion parameter.

Nature	GVD /$fs^2 m^{-1}$	D_λ/ps(nm km)$^{-1}$	Pulse delay/fs
Air (mp)	1.0734	0.830 83	12.5(2500)
m. subst.	$-3 \cdot 10^4$	20	20
dm (mp)	~30 − 100/L	...	<1 (<200)
NGVD m.	~ −400/L	...	>−4
Metal m.	Very low	...	...

light source yields a theoretical reflection value of 97.07%, a transmission of 0.86% and an absorption of 2.07%.[29] The thickness of the fused silica was 50 mm. All values can vary about 0.1% within the wavelength range between 1500 nm and 1600 nm. The resulting cavity finesse is approximately 166.[23]

To decrease the effects of thermal expansion, the cavity mirror's layers were made on fused silica substrates of 12.3 mm diameter. The mirrors were coated homogeneously by the deposition technique on the RF magnetron sputtering[30] with silver over the 11 mm diameter of each substrate. We used silver target with 99.95% purity and 150 mm in diameter. A working gas of argon was used under the deposition pressure of 0.24 Pa with forward RF power of 150 W at 13.56 MHz. The coating thickness was measured by Talystep profilometer as (40.2 ± 0.9) nm.

D. Cavity length control

The control electronics used for the cavity length control are shown in Fig. 3. The control electronics for locking the cavity length to the repetition frequency of FPC used the derivative spectroscopy detection. The signal zero intersection corresponded to the transmitted mode resonance. The intensity of optical signal detected by the photodetector (PD), converted by analog-to-digital converter (ADC) and input into the servo-loop after the intensity signal was mixed synchronously with 1 kHz digital signal generated on the direct digital synthesizer (DDS). Thus we directly generated the digitised error signal in the waveform that represents the first derivative of the optical intensity. The servo-loop proportional integral derivative (PID) controller provides the calculation of the appropriate value for the displacement of the PZT actuator. This value is converted by the digital-to-analog converter 1 (DAC1) with non-inverted and digital-to-analog converter 2 (DAC2) with inverted polarity to analog voltage representations. The output voltage from DAC1 and DAC2 are amplified by two high-voltage amplifiers HVA1 and HVA2, which drive the bipolar PZT actuator in the bridge setup. Finally the PZT actuator was driven by the 1 kHz sinusoidal voltage thereby modulating the length of the cavity. Signal conditioning was necessary to achieve the sufficient displacement of the cavity length by PZT actuator and to avoid a possible damage of PZT if the absolute maximum value of applied voltage was exceeded.
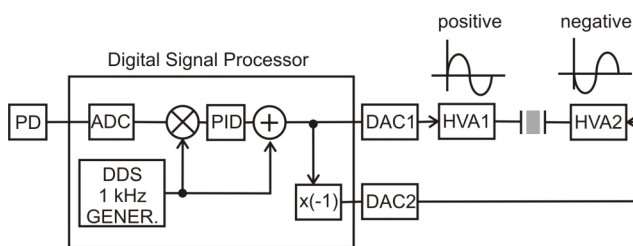

FIG. 3. Scheme of the digital signal processor and electronic loop for the PZT voltage control: PD—photodetector, PZT control—piezo-electric transducer, DAC1, DAC2—digital-analog converters, HVA1, HVA2—high voltage amplifiers, ADC—analog-digital converter, PID—PID control set, DDS—direct digital synthesizer.

IV. RESULTS

The main goal in the construction of the Fabry-Perot cavity was to maintain the cavity mirror distance fixed to the desired transmission mode and fulfill Eq. (2), as discussed in Section III. Because we have chosen commercial mirror holders based on standard materials, the coarse position of mirrors was found manually with the precision kinematic mounts and the long-term length stability of the FPC was controlled by PZT transducer control loop. The search for the resonant modes has been done with full PZT displacement. Each of high voltage amplifiers HVA1 and HVA2 had maximal output lift up to ±140 V so the PZT actuator can be driven up to ±280 V (or 560 V peak-to-peak). Taking into account the measured sensitivity of PZT has been 3.96 nm/V the maximal lift corresponds to ~2200 nm displacement of the FPC.

A. Transmission spectrum of the cavity

To study the transmission spectrum of the cavity, the first step was to couple the narrow tunable laser diode working at 1540 nm (ORION laser module) to the FC/APC fiber input and hence directly to the collimator in front of the mode-matching lenses and the cavity. The position of the cavity mirrors and the mode-matching lenses were found using Eq. (2) and coarse mechanical alignment. The cavity was aligned and locked to the TEM_{00} mode of the laser by the first derivative technique using the ramp length modulation of the piezo-ceramic transducers on the flat mirror holder. The alignment for TEM_{00} mode is represented by the PZT voltage-intensity plot shown in Fig. 4. Subsequently the optical frequency comb laser working in the range from 1500 nm to 1600 nm was directed to the fiber collimator as shown in Fig. 1. The light from the laser comb passed through the same single mode fiber onto the same fiber collimator as the single mode laser (ORION laser module). Because the cavity was already aligned for the 1540 nm single mode laser, it only needed to be precisely positioned to the position where it matched the condition in Eq. (2). The record of the scan of FPC length with the frequency comb laser is shown in Fig. 4. The theory[31]
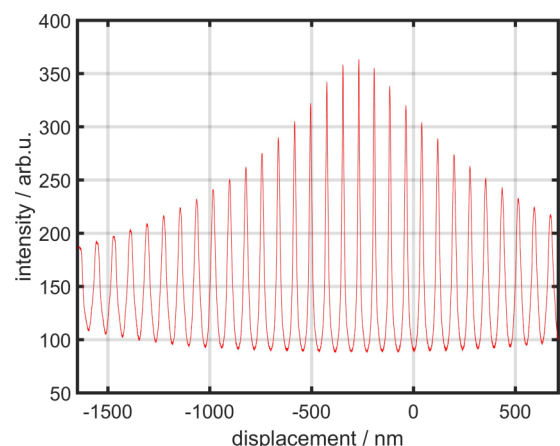

FIG. 4. Fabry-Perot output filtering signal representing the purity of TEM_{00} on 100 MHz frequency comb in the cavity with PZT scan over its dynamic range.

predicts one comb mode for the displacement ΔL,

$$\Delta L = \frac{f_{\text{rep}} \cdot \lambda_{\text{c}}}{2 \cdot \nu_{\text{FSR}}} = 78 \text{ nm}, \tag{4}$$

where λ_{c} is the central wavelength of the comb. We observed 30 comb lines in the cavity that corresponded to 2315 nm in our measurement and 2340 nm according to theoretical models in Eq. (4), with a reliability of 1%. Therefore the cavity was well aligned to TEM_{00} mode.

B. Beat-note frequency spectrum

The effectiveness of repetition frequency multiplication has been measured by two separate methods. The first method was the direct measurement with the commercially available infra-red fast photodiode FPD310, MenloSystems GmbH working in the range 10-1000 MHz. The beat-note frequency spectrum has been recorded with RF spectrum analyzer Rigol DSA1030. The measurement has been done with and without the external FPC. For this measurement, auxiliary silver mirrors were added in the direct cavity filter light represented by the dashed line in Fig. 1. Comparison between the initial comb spectrum and filtered external FPC spectrum is shown in the Fig. 5. We have intentionally chosen the highest resolution bandwidth and similar video bandwidth and cutoff the DC part of the spectra. The initial RF spectra, Fig. 5 (left), were attenuated by 30 dB. It should be noted that the photodiode FPD310 cannot measure beat frequencies beyond the 1.4 GHz limit, thus this method cannot confirm the higher harmonics of the signal. The measurement showed that the method was effective generating 1 GHz signal from the initial 100 MHz repeated spectrum.

C. VIPA spectrometer

In addition to the measurements using the fast photodiode, a second method for studying the effect of the external cavity filtering on spectral data was used. Here, we used the Virtually Imaged Phased Array (VIPA) spectrometer.[13] The VIPA owes its name to the existence of multiple virtual sources contributing to a wavelength dependent transmission in certain directions.[17] It acts, similar to grating, as an angular
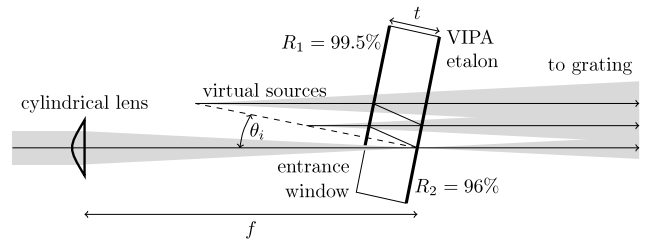

FIG. 6. Creation of virtual sources in a VIPA etalon.

disperser spatially separating the different lasing modes. The advantage of the method is that it can observe high repetition frequency values and directly determine the mode spacing of the optical comb avoiding any misinterpretation of the laser light repetition frequency. The only drawback is the need for the precise positioning of each optical element and the following correct data treatment. The detection part of the VIPA spectrometer in our experimental setup (Fig. 1) consisted of focal optics (lenses), VIPA etalon, grating and detector. An incoming collimated beam is focused by a cylindrical lens on the back end of the VIPA etalon from Precision Photonics, S-LAA71, which consists of a glass plate of thickness $t = 1.75$ mm, with reflective coating on both sides. The entrance side has a reflection coefficient of $R_1 = 99.5\%$ and the output side has a reflection coefficient of $R_2 = 96\%$. A small entrance window is left uncoated on the entrance side of the VIPA etalon to allow for incoupling of laser light as can be seen in Fig. 6. A grating was used as post-disperser (Spectrogon UK, G1100 31 × 50 × 10 NIR, 1100 lines/mm). The FSR of the VIPA depends on the etalon thickness and the incidence angle of the light. The incidence angle is usually very low (≈ 0), thus we can write

$$\text{FSR} \approx \frac{c}{2n_{\text{e}}t}, \tag{5}$$

where t is the thickness and n_{e} the refractive index of the etalon.[17] After being dispersed by the etalon and the grating, the light is imaged on an infra-red camera (XenICs XEVA-FPA-1.7-640) using a lens.

The full spectrum is contained in adjacent lines representing one FSR of 50 GHz each. With a resolution of 680 MHz, the mode spacing of the frequency comb without cavity
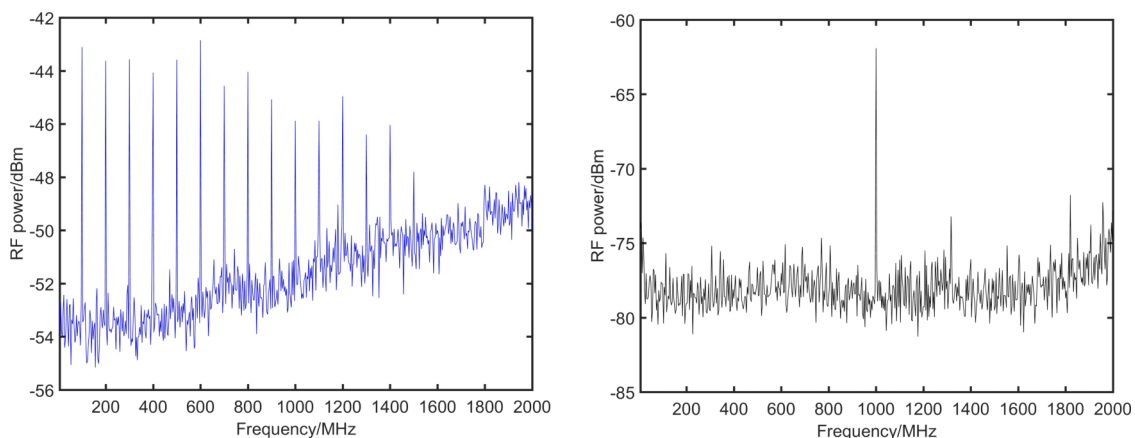

FIG. 5. RF spectrum of the optical frequency comb before filtering (left) and after filtering with external FPC (right).
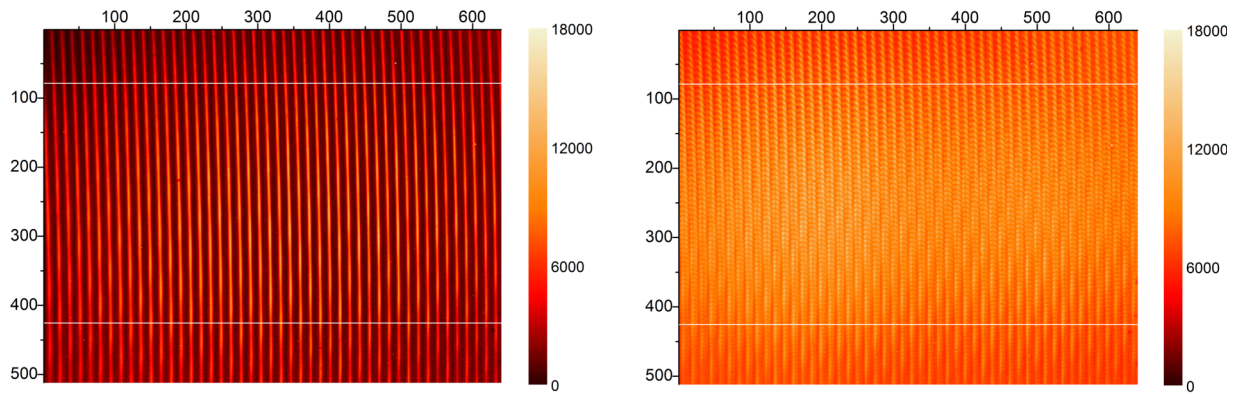
FIG. 7. VIPA spectrum of the optical frequency comb with central wavelength at 1560 nm without (left) and with (right) external FPC filtering cavity.

filtering cannot be resolved. When applying cavity filtering, the mode spacing gets stretched to 1 GHz, i.e., well within the resolution limits of the spectrometer. This enables long distance measurements.[18]

The VIPA was calibrated using a single-mode laser, the ORION module, which emits light seen as single spot reappearing on the vertical spectral line after one VIPA FSR. Thus an absolute wavelength comparison as well as the length of the FSR in pixels can be determined. Fig. 7 (left figure) represents the VIPA image for optical frequency comb without external cavity filtering. As we can see the VIPA's FSR resolution of 680 MHz is not enough to distinguish between two adjacent modes of the optical frequency comb.

A clear distinction between the lasing modes of the cavity-filtered frequency comb can be made as seen in Fig. 7 (right figure), which was impossible prior to the application of the filter. The mode spacing was measured to be (980 ± 40) MHz and was obtained by counting the peak numbers per line. The error arises from the uncertainty of determining the FSR on the camera. The results of the VIPA measurement matched those obtained by the fast photodiode.

V. CONCLUSION

In this work, we presented the filtering of the repetition frequency of the 100 MHz infrared optical frequency comb by external Fabry-Perot cavity for application in long distance measurements. We designed the cavity based on the thin layer silver mirrors and the commercially available optical holder system. By using two methods, we have verified that the resulting repetition frequency increased to 1 GHz making it feasible to use for field measurements along with fiber based compact frequency combs.

[1]N. R. Newbury, "Searching for applications with a fine-tooth comb," Nat. Photonics **5**, 186–188 (2011).

[2]S. A. Diddams, "The evolving optical frequency comb (invited)," J. Opt. Soc. Am. B **27**(11), B51–B62 (2010).

[3]M. T. Murphy, T. Udem, R. Holzwarth, A. Sizmann, L. Pasquini, C. Araujo-Hauck, H. Dekker, S. D'Odorico, M. Fischer, T. W. Hänsch, and A. Manescau, "High-precision wavelength calibration of astronomical spectrographs with laser frequency combs," Mon. Not. R. Astron. Soc. **380**, 839–847 (2007).

[4]A. J. Benedick, G. Chang, J. R. Birge, L.-J. Chen, A. G. Glenday, C.-H. Li, D. F. Phillips, A. Szentgyorgyi, S. Korzennik, G. Furesz, R. L. Walsworth, and F. X. Kärtner, "Visible wavelength astro-comb," Opt. Express **18**(18), 19175–19184 (2010).

[5]M. J. Thorpe, D. Balslev-Clausen, M. S. Kirchner, and J. Ye, "Cavity-enhanced optical frequency spectroscopy: Application to human breath analysis," Opt. Express **16**(4), 2387–2397 (2008).

[6]J. Ye, "Absolute measurement of a long, arbitrary distance to less than an optical fringe," Opt. Lett. **29**(10), 1153–1155 (2004).

[7]M. Cui, M. G. Zeitouny, N. Bhattacharya, S. A. van den Berg, H. P. Urbach, and J. J. M. Braat, "High-accuracy long-distance measurements in air with a frequency comb laser," Opt. Lett. **34**(13), 1982–1984 (2009).

[8]K. Minoshima and H. Matsumoto, "High-accuracy measurement of 240-m distance in an optical tunnel by use of a compact femtosecond laser," Appl. Opt. **39**(20), 5512–5517 (2000).

[9]I. Coddington, W. C. Swann, L. Nenadovic, and N. R. Newbury, "Rapid and precise absolute distance measurements at long range," Nat. Photonics **3**, 351–356 (2009).

[10]J. Lee, Y.-J. Kim, K. Lee, S. Lee, and S.-W. Kim, "Time-of-flight measurement with femtosecond light pulses," Nat. Photonics **4**, 716–720 (2010).

[11]K.-N. Joo and S.-W. Kim, "Absolute distance measurement by dispersive interferometry using a femtosecond pulse laser," Opt. Express **14**(13), 5954–5960 (2006).

[12]M. Cui, M. G. Zeitouny, N. Bhattacharya, S. A. van den Berg, and H. P. Urbach, "Long distance measurement with femtosecond pulses using a dispersive interferometer," Opt. Express **19**, 6549–6562 (2011).

[13]S. A. Diddams, L. Hollberg, and V. Mbele, "Molecular fingerprinting with the resolved modes of a femtosecond laser frequency comb," Nature **445**, 627–630 (2007).

[14]L. Nugent-Glandorf, T. Neely, F. Adler, A. J. Fleisher, K. C. Cossel, B. Bjork, T. Dinneen, J. Ye, and S. A. Diddams, "Mid-infrared virtually imaged phased

array spectrometer for rapid and broadband trace gas detection," Opt. Lett. **37**(15), 3285–3287 (2007).

[15] B. Bernhardt, A. Ozawa, P. Jacquet, M. Jacquey, Y. Kobayashi, T. Udem, R. Holzwarth, G. Guelachvili, T. W. Hänsch, and N. Picqué, Nat. Photonics **4**, 55–57 (2010).

[16] J. Mandon, G. Guelachvili, and N. Picqué, "Fourier transform spectroscopy with a laser frequency comb," Nat. Photonics **3**, 99–102 (2009).

[17] S. Xiao and A. Weiner, "2D wavelength demultiplexer with potential for ≤1000 channels in the C-band," Opt. Express **12**, 2895–2902 (2004).

[18] S. A. van den Berg, S. T. Persijn, G. J. P. Kok, M. G. Zeitouny, and N. Bhattacharya, "Many-wavelength interferometry with thousands of lasers for absolute distance measurement," Phys. Rev. Lett. **108**, 183901 (2012).

[19] H. Jiang, J. Taylor, F. Quinlan, T. Fortier, and S. A. Diddams, "Noise floor reduction of an Er:fiber laser-based photonic microwave generator," IEEE Photonics J. **3**, 1004–1012 (2011).

[20] F. Adler, K. Moutzouris, A. Leitenstorfer, H. Schnatz, B. Lipphardt, G. Grosche, and F. Tauser, "Phase-locked two-branch erbium-doped fiber laser system for long-term precision measurements of optical frequencies," Opt. Express **12**(24), 5872–5880 (2004).

[21] T. Sizer II, "Increase in laser repetition rate by spectral selection," IEEE J. Quantum Electron. **25**(1), 97–103 (1989).

[22] J. Mildner, K. Meiners-Hagen, and F. Pollinger, "Dual-frequency comb generation with differing GHz repetition rates by parallel Fabry-Perot cavity filtering of a single broadband frequency comb source," Meas. Sci. Technol. **27**, 074011 (2016).

[23] J. R. Lawall, "Fabry-Perot metrology for displacements up to 50 mm," J. Opt. Soc. Am. A **22**, 2786–2798 (2005).

[24] G. Bönsch and E. Potulski, "Measurement of the refractive index of air and comparison with modified Edlén's formulae," Metrologia **35**, 133–139 (1998).

[25] P. E. Ciddor, "Refractive index of air: New equations for the visible and near infrared," Appl. Opt. **35**, 1566–1573 (1996).

[26] R. Szipöcs, "Dispersive properties of dielectric laser mirrors and their use in femtosecond pulse lasers," Ph.D thesis, SZTE TTK Szeged, Hungary, 2000.

[27] W. H. Knox, N. M. Pearson, K. D. Li, and C. A. Hirlimann, "Interferometric measurements of femtosecond group delay in optical components," Opt. Lett. **13**(7), 574–576 (1988).

[28] M. N. Polyanskiy, Refractive index database, http://refractiveindex.info, (accessed 30 February 2016).

[29] A. D. Rakić, A. B. Djurišic, J. M. Elazar, and M. L. Majewski, "Optical properties of metallic films for vertical-cavity optoelectronic devices," Appl. Opt. **37**, 5271–5283 (1998).

[30] A. V. Tikhonravov, M. K. Trubetskov, J. Hrdina, and J. Sobota, "Characterization of quasi-rugate filters using ellipsometric measurements," Thin solid films **277**(1-2), 83–89 (1996).

[31] S. Kyriacou, "Design and characterisation of a femtosecond enhancement cavity," Diploma thesis, Imperial College London, 2010.